CHINESE OPTICS LETTERS | Fast Track

Vol. 21, No. 12 | December 2023

Observation of topological rainbow in non-Hermitian systems

Cuicui Lu (路翠翠)[1*,†], Wen Zhao (赵 闻)[1,†], Sheng Zhang (张 胜)[2,†], Yanji Zheng (郑焱基)[1], Chenyang Wang (王晨阳)[3], Yaohua Li (李耀华)[3], Yong-Chun Liu (刘永椿)[3], Xiaoyong Hu (胡小永)[4**], and Zhi Hong Hang (杭志宏)[2***]

[1] Key Laboratory of Advanced Optoelectronic Quantum Architecture and Measurements of Ministry of Education, Beijing Key Laboratory of Nanophotonics and Ultrafine Optoelectronic Systems, School of Physics, Beijing Institute of Technology, Beijing 100081, China

[2] School of Physical Science and Technology, Provincial Key Laboratory for Thin Films and Institute for Advanced Study, Soochow University, Suzhou 215006, China

[3] State Key Laboratory of Low-Dimensional Quantum Physics, Department of Physics, Frontier Science Center for Quantum Information, Tsinghua University, Beijing 100084, China

[4] State Key Laboratory for Mesoscopic Physics & Department of Physics, Collaborative Innovation Center of Quantum Matter & Frontiers Science Center for Nano-optoelectronics, Beijing Academy of Quantum Information Sciences, Peking University, Beijing 100871, China

*Corresponding author: cuicuilu@bit.edu.cn

**Corresponding author: xiaoyonghu@pku.edu.cn

***Corresponding author: zhhang@suda.edu.cn

Received August 14, 2023 | Accepted August 18, 2023 | Posted Online November 3, 2023

Topological photonic states have promising applications in slow light, photon sorting, and optical buffering. However, realizing such states in non-Hermitian systems has been challenging due to their complexity and elusive properties. In this work, we have experimentally realized a topological rainbow in non-Hermitian photonic crystals by controlling loss in the microwave frequency range for what we believe is the first time. We reveal that the lossy photonic crystal provides a reliable platform for the study of non-Hermitian photonics, and loss is also taken as a degree of freedom to modulate topological states, both theoretically and experimentally. This work opens a way for the construction of a non-Hermitian photonic crystal platform, will greatly promote the development of topological photonic devices, and will lay a foundation for the real-world applications.

Keywords: topological rainbow; non-Hermitian photonics; photonic crystal; slow-light effect.
DOI: 10.3788/COL202321.123601

1. Introduction

Topological photonics, which combines photonics, geometric topology, and condensed matter physics, provides a new and robust platform to study the interactions between light and matter due to the protection of topology, and has triggered various physical phenomena and prospective applications[1–7]. In recent years, topological photonic devices have attracted intense attention due to their unique properties of unidirectional propagation and immunity to disorders[8–12]. "Rainbows," which can separate and enable different frequencies of light to propagate and stop at different positions accompanied by different group velocities, have been realized in various optical systems[13–16]. Then the topology is introduced into the rainbow device to form the topological rainbow device with the advantage of robustness, which has been realized in various Hermitian systems[17–20].

Unfortunately, the Hermitian system is ideal and rare, since many of the optical systems are non-Hermitian in the real world, especially for most loss systems. Loss is ubiquitous—an inherent characteristic of most materials. How to deal with and utilize loss is vital in the development of topological photonic devices. The non-Hermitian systems have many novel and rich physics that remain to be explored and have broad application prospects in the development of photonic devices[21–25]. However, most of the non-Hermitian systems, to be described using non-Hermitian operators, which have complex and elusive physics, are difficult to study[26–32]. To date, it is still a great challenge to realize the observation of topological rainbow in non-Hermitian systems due to lack of experimental schemes.

In this work, we propose a method to realize the topological rainbow in non-Hermitian photonic crystals (PCs). The topological photonic states are generated at the interface of two PCs, where one PC is undeformed, and the other PC has a translational value of part of one lattice. Loss has been demonstrated as an effective mean to tune the topological state of the different

frequencies to propagate into different positions, which provides a new degree of freedom to design topological rainbow devices. In addition, loss can also directly contribute to construction of topological photonic states accompanied by periodic translational parameters of lattices in non-Hermitian systems. Only requiring a PC with bandgap, the realization of such a topological rainbow in non-Hermitian systems is general and of great convenience because no external magnetic field is needed, with no limitations for symmetries and lattice types. As for experimental verifications, the microwave PCs with finely tuned graded tangential loss have been fabricated and assembled, and the near-field measurements of the electric field have been performed. Obvious topological rainbows have been observed in non-Hermitian systems in an operation band range from 7.725 to 8.355 GHz. Different frequencies of topological photonic states propagate and stop at different positions because of the gradually decreasing group velocities. This work provides an effective method to realize topological photonic devices in non-Hermitian systems and will promote the practical applications of topological states, especially for slowing light, photon buffers, and broadband optical information processing.

2. Results

2.1. Construction and design of the topological rainbow

First, the basic idea of constructing the topological rainbow in a non-Hermitian system is introduced. Take the simple square lattice of PC as an example. A two-dimensional (2D) PC structure with loss is proposed, as shown in Fig. 1(a), comprising square lattices of dielectric cylinders ($n = 2.4 + n_I i$) embedded in the air ($n = 1$). The imaginary part $n_I i$ of the refractive index represents the lossy nature of the dielectric materials. The topological photonic states can be generated at the interface formed by an undeformed lattice and its counterpart with a translational distance of ξ along the x direction. Our proposed topological photonic structure has the same translational distance ξ but different n_I for different rows, in which ξ is fixed at $0.5a$ and n_I is set to be from 0 to 1 along the y direction. Topological photonic states can be modulated by loss to form a topological rainbow at the interface of PCs, where states with different frequencies can propagate and stop at different positions.

Here the Zak phase $\theta^{(\mathrm{Zak})}_{m,k_y,n_I}(k_x)$ is calculated to identify the topological properties of structures. The Berry curvature of each band is obtained by analyzing the numerically calculated eigen electric field distributions of PCs using the finite-element method (FEM). The eigenstate $n_m(k_x, k_y, n_I)$ in the momentum space of the mth band can be labeled by the Bloch wave vector (k_x, k_y) and the imaginary part of the refractive index n_I. For a fixed k_y, the link variable $U_{m,k_y,n_I}(k_x)$ and the Zak phase $\theta^{(\mathrm{Zak})}_{m,k_y,n_I}(k_x)$ of the band m can be calculated as[17,18,33–35]

$$U_{m,k_y,n_I}(k_x) = \frac{\langle n_{m,k_y,n_I}(k_x) | n_{m,k_y,n_I}(k_x + \delta k_x)\rangle}{|\langle n_{m,k_y,n_I}(k_x) | n_{m,k_y,n_I}(k_x + \delta k_x)\rangle|}, \tag{1}$$

$$\theta^{(\mathrm{Zak})}_{m,k_y,n_I}(k_x) = -\mathrm{Im}\left(\ln\left(\prod \langle U_{m,k_y,n_I}(k_x) | U_{m,k_y,n_I}(k_x + \delta k_x)\rangle\right)\right). \tag{2}$$

Although the phases for the right and left eigenvectors are different in the non-Hermitian system, if we choose the same

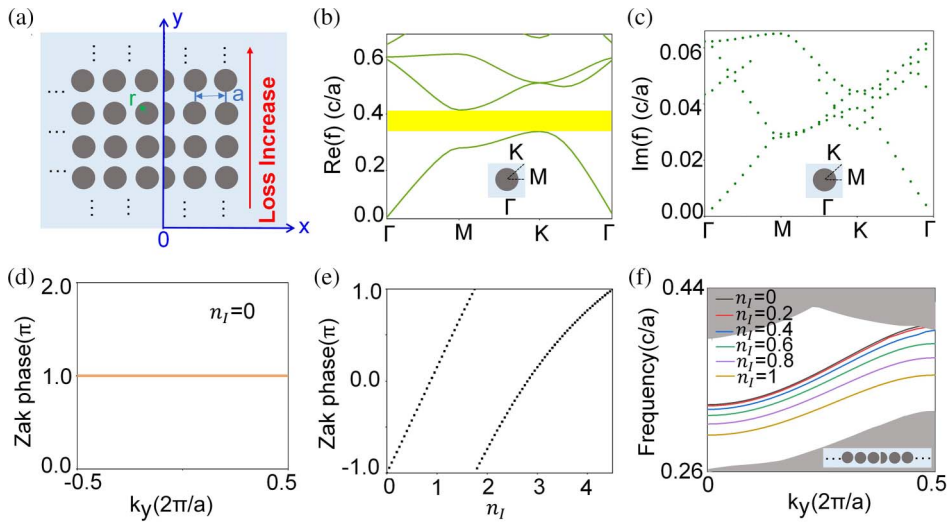

Fig. 1. Geometric structure, bulk bands, Zak phase, and the interface states. (a) Non-Hermitian 2D PC structure with square lattices of dielectric column ($n = 2.4 + n_I i$) embedded in the air ($n = 1$), in which different rows of the dielectric materials have different loss factors n_I. a is the lattice constant, and the radius r is $0.27a$. (b), (c) Real and imaginary parts of dispersion bands of the 2D PC in TM mode, respectively, and n_I is 0.3. The inset is the corresponding unit cell. (d) Calculated values of the Zak phase for the translational lattice at the right of the structure shown in (a), which shows the topological properties of our proposed structure; (e) evolution of the Zak phase for the first bulk band as a function of loss factor n_I; (f) dispersion curves of different super unit cells, as shown in the inset. Each color curve corresponds to different loss factors n_I.

eigenvectors for the states at the same locations, it does not affect the calculation results[35].

Taking the transverse magnetic (TM) mode for example, whose electric field is along the z direction, the real and imaginary parts of calculated dispersion relations of the unit cell are shown in Figs. 1(b) and 1(c), respectively. For the bulk energy bands under the bandgap, the calculated Zak phase of the translational lattice as a function of k_y in the momentum space is shown in Fig. 1(d), where the Zak phase always take an integer quantized value π when $n_I = 0$, which verifies its topological nature[33,34,36]. The Zak phase of this band as a function of n_I is also calculated, where the value of n_I ranges from 0 to 4.5, as shown in Fig. 1(e). The Zak phase is $-\pi$ when the loss is 0 and evolves continuously along with the modulation of loss due to the breaking of chiral symmetry (the same phenomenon is also stated in Ref. [35]). In the whole evolution process, it always satisfies the topological property[33,35]. Therefore, our proposed structure, which has the same translational distances and different losses for different rows, is topologically satisfied in the non-Hermitian systems.

We calculate the energy bands of the supercell, as shown in Fig. 1(f), where the x direction is exerted by the scattering boundary condition, and for the y direction it is the periodic boundary condition. It is obvious that different loss can generate different interface states with different frequencies, which is used to form the topological rainbow. The group velocities of the topological interface states can be used to understand the underlying physics for the formation of the topological rainbow. More calculation details of group velocity are shown in Supplementary Material Section 1[33]. The distributions of group velocities of the interface states are plotted as a function of frequency and the parameter n_I in Fig. 2(a). The dark regions are the areas without interface states, and in the bright region, the interface states exist, where the color depth indicates the magnitude of group velocities of the interface states. The green dashed lines mark the boundaries of the three regions and are zero group velocity lines. When n_I changes, the frequency of interface states with zero group velocity can also be changed, and thus the topological rainbow is formed.

We thus can explore the topological rainbow in non-Hermitian systems. Considering a PC with gradually increasing loss distribution for different rows, the propagating topological photonic states will be slowed down to stop at a certain position where the corresponding group velocity of the topological state along the interface is zero, where the waves eventually "stop" there in principle. Figure 2(b) shows the electric field intensity and the Poynting vector power flow distributions of the topological rainbow as functions of distance Y and frequency. Figures 2(c) and 2(d) show the electric intensity and Poynting vector power flow distributions along the interface between undeformed and deformed structures, respectively, and the topological states with different frequencies are stopped at different spatial positions along the propagation direction to form a topological rainbow in the non-Hermitian PC. Due to the similar role played by gain and loss in the Hamiltonian, it is feasible that a similarly slow-light effect can also occur in a system with gain in materials. We also calculate and discuss the linear bandgap in the complex plane and find that the bandgap still

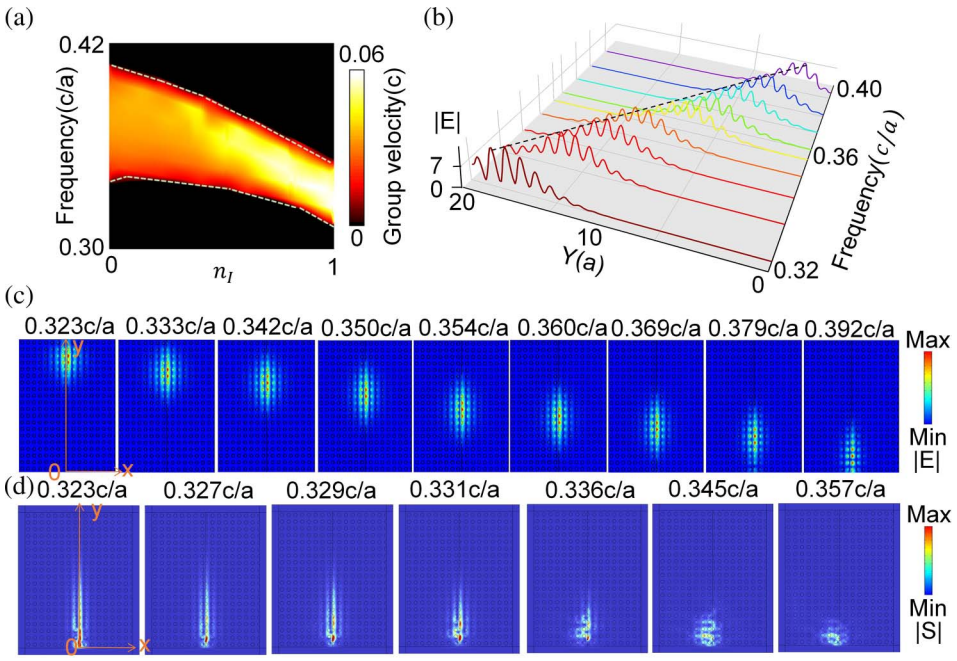

Fig. 2. Non-Hermitian topological rainbow in the interface of two kinds of PCs. (a) Group velocity contour as a function of n_I and frequency; (b) magnitude of electric field distributions of all interface states; Y represents the distance of any positions along the y direction, and the fluctuation of the curve shows the magnitude of **E**. (c) |**E**| field distribution of the topological rainbow trapping phenomenon of nine topological states shown in (b); (d) Poynting vector power flow |**S**| distribution of the topological rainbow trapping phenomenon.

exists in a large range of loss, which ensures the feasibility of our work (Supplementary Material Section 2).

2.2. Samples preparation and experimental verification

In the experiment, we construct composite structures composed of dielectric material (alumina, with relative permittivity of 7) surrounded by lossy material with different thicknesses. As can be seen in Fig. 3(a), alumina cylinders of radius $r = 3.75$ mm and height of 8 mm are arranged into square arrays with lattice constant $a = 13$ mm. The finite height sample is sandwiched between two parallel metallic plates (see Section 4 for details), and this is a perfect platform to explore 2D TM PC properties. Similar samples and experimental setups have been used to realize various topological photonics properties[37–39], which further demonstrate the feasibility and reliability of such a system. A photonic bandgap will open between 7.5 and 8.5 GHz for this 2D dielectric PC, and the Zak phase-induced deterministic interface state appears in this common bandgap if we assemble a 2D PC with its counterpart shifted by half a lattice constant[37]. Electromagnetic interference (EMI) shielding material (in dark blue) is used to surround the PC structures to absorb unwanted scattering. Vertically, 10 arrays each are considered to guarantee the confinement of interface states. Though alumina is lossless at microwave frequencies, we can wrap EMI shielding materials [black in Figs. 3(a) and 3(b)] of different thickness d, with a measured permittivity of $1.1 + 0.4i$ in the frequency range of a common bandgap, to tune loss locally in this 2D PC.

To visualize the non-Hermitian topological rainbow, given the limitation of our translational stage, horizontally, a 30-layer sample is prepared. We use the same wrapped PC structure for every five layers, and the bottom part is unwrapped alumina cylinders. The other thicknesses d of wrapping EMI shield materials are 0.55, 1, 1.25, 1.45, and 1.75 mm, and d increases along the forward direction of the y axis. Such core-shell structures with increased wrapping thicknesses shall be considered as cylinders with the increasing radii and imaginary part of permittivity, but the decreasing real part of permittivity. The measured electric field amplitude distributions $|\mathbf{E}|$ can be found in Fig. 3(d). With an increase of wrapping thickness (increasing loss), as in the distributions in Fig. 2(a), the frequency of zero group velocity of interface state redshifts. Thus, the electromagnetic fields incident from the bottom tend to stop "earlier" at higher frequencies, as shown clearly in microwave experiments. We also carried out brute force FEM simulations considering the exact experimental setup [with results shown in Fig. 3(c)]. Not only can nearly identical field distributions be found, but also frequencies between experimental and simulation results, showing a nearly consistent topological rainbow. Time domain calculations for different frequencies of topological states are carried out (Supplementary Material Section 3) and corresponding fast Fourier transform (FFT) calculations are also performed, which are in accordance to the results of the group velocities.

The robustness of the topological rainbow for square lattices is verified by introducing dislocations into the PC structure. As five different types of wrapped alumina cylinders are introduced, and each cylinder duplicates for five layers in the experiments,

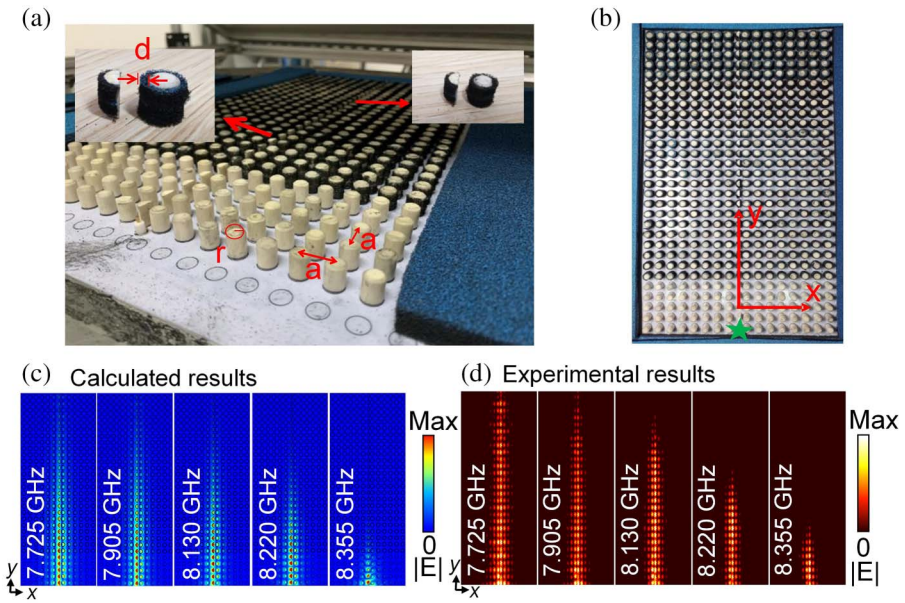

Fig. 3. Samples and experimental setup; calculated and measured topological rainbow for square lattices in non-Hermitian systems. (a), (b) Proposed experimental structure consists of a square lattice PC array of wrapped alumina cylinders with a relative permittivity of 7. The thicknesses of lossy materials (sponges, the measured permittivity is $1.1 + 0.4i$) for each group increase gradually from bottom to top. (c), (d) Simulated and experimentally measured $|\mathbf{E}|$ of topological rainbow in non-Hermitian systems.

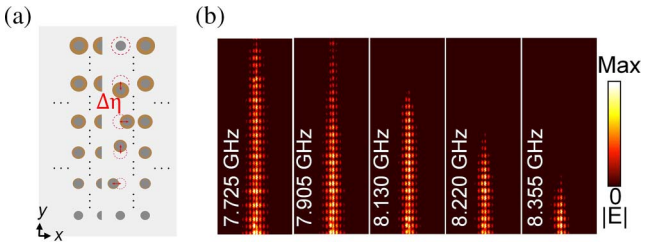

Fig. 4. Robustness of topological rainbow. (a) Schematic of the PC for square lattices with defects; (b) corresponding measured electric field amplitude distributions |**E**|; the appearance of the topological rainbow has been slightly affected by disorders, which shows the robustness of our structures.

five different types of dislocations are introduced to our proposed square lattice structures, as depicted in Fig. 4(a). In simulations, all these dislocation distributions have almost no influence on the appearance of the topological rainbow. As shown in Fig. 4(b), experimentally we only observe slight electromagnetic field distribution differences compared to Fig. 3(d). The experimental results prove that topological rainbow structures show great robustness for lattices of any type.

Loss normally means something bad in optical devices. What if the loss can be used to control the property of optical devices? Group velocity plays a major physical role in the topological rainbow, and local loss can be used to tune the corresponding group velocity. Combining these two factors, the loss can be used to control the topological rainbow property. We consider three different cases of wrapping thickness (0, 0.55, 1, 1.25, 1.45, and 1.75 mm; 0.55, 1, 1.25, 1.45, 1.75, and 2.25 mm; 1, 1.25, 1.45, 1.75, 2.25, and 2.5 mm). By rearranging the wrapping thickness distributions, we can manipulate the position at which the light stops. The induced topological state at the structure with wrapping thickness of $d = 1.45$ mm shall have zero group velocity at 8.13 GHz, while for a different wrapping thickness, the corresponding group velocity shall be different. Thus, light stops when propagating to that region with zero group velocity. The topological photonic state of the same frequency can be tuned to propagate to different positions when the loss is changed, as shown in Fig. 5, which has verified the degree of freedom for tunability function of loss.

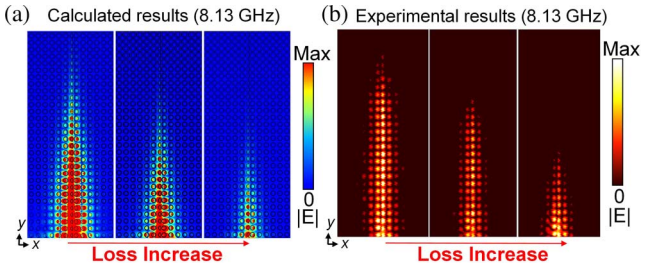

Fig. 5. Tuning topological rainbow. (a) Calculated electric field |**E**| distributions with different wrapping thickness of lossy materials at frequency 8.13 GHz; (b) experimentally measured electric field amplitude |**E**| distributions at frequency 8.13 GHz. Under the different loss distributions, the interface state stops at different spatial positions.

3. Conclusion

In conclusion, the topological rainbow has been observed in non-Hermitian systems for what we believe is the first time. The construction of topological photonic states has good universality, which can be realized easily only if the PC has a bandgap and is not restricted by symmetries and lattice types. The introduction of graded loss into materials, which is achieved by wrapping the lossless dielectric cylinders with lossy materials of different thicknesses, plays a key role in engineering the group velocity of the topological photonic states. Obvious topological rainbow phenomena have been observed in non-Hermitian systems in a broadband range from 7.725 to 8.355 GHz. The devices allow topological photonic states with different frequencies to propagate and stop at different spatial locations. This work provides an effective method to construct and modulate materials with different loss and topological photonic states with multiple frequencies in non-Hermitian systems, which will promote the practical application of topological photonic devices in the real world.

4. Methods

Theoretical calculations: The data of eigen electromagnetic field distributions are calculated by COMSOL Multiphysics software, and then the Zak phase is calculated by MATLAB software. The bands of bulk states and interface states, as well as the intensity distribution of the topological rainbow, are both calculated by the FEM of COMSOL Multiphysics software.

Experimental measurements: With TM polarization where the electric field is parallel to the cylinder axis explored, the sample is contained inside a parallel-plate waveguide made with two large flat metallic plates. The source antenna, the PC structures, and EMI shielding materials are assembled on the bottom plate, and the probing antenna is fixed through a hole on the top metallic plate. Both the source and probing antenna are connected to our Agilent E5071C vector network analyzer for data acquisition. The bottom plate, along with the samples, is mounted on a computer-controlled xy translational stage and thus the time harmonic electric field distributions can be measured spatially from point to point. The distance between the top metallic plate and the bottom plate is fixed at 8.5 mm, which is much smaller than half of the wavelength of the incident microwave (~7.5 GHz, approximately 40 mm), and thus the electric field is perpendicular to the metallic plates. This parallel metallic waveguide system is adopted only to deduce the height of the sample, and all the physics revealed theoretically for 2D TM PCs remain unchanged.

Acknowledgement

This work was supported by the National Natural Science Foundation of China (Nos. 12274031, 12274315, 92050110, 11734001, 91950204, and 92150302), the Priority Academic Program Development of Jiangsu Higher Education

Institutions (PAPD), the National Key Research and Development Program of China (No. 2018YFB2200403), the Beijing Institute of Technology Research Fund Program for Teli Young Fellows, and the Beijing Institute of Technology Science and Technology Innovation Plan Innovative Talents Science and Technology Funding Special Plan (No. 2022CX01006).

†These authors contributed equally to this work.

References and Note

1. L. Lu, J. D. Joannopoulos, and M. Soljačić, "Topological photonics," Nat. Photonics **8**, 821 (2014).
2. F. D. Haldane and S. Raghu, "Possible realization of directional optical waveguides in photonic crystals with broken time-reversal symmetry," Phys. Rev. Lett. **100**, 013904 (2008).
3. F. D. Haldane and S. Raghu, "Experimental observation of large Chern numbers in photonic crystals," Phys. Rev. Lett. **115**, 253901 (2015).
4. P. Titum, N. H. Lindner, M. C. Rechtsman, and G. Refael, "Disorder-induced Floquet topological insulators," Phys. Rev. Lett. **114**, 056801 (2015).
5. M. C. Rechtsman, J. M. Zeuner, Y. Plotnik, Y. Lumer, D. Podolsky, F. Dreisow, S. Nolte, M. Segev, and A. Szameit, "Photonic Floquet topological insulators," Nature **496**, 196 (2013).
6. J. W. Dong, X. D. Chen, H. Zhu, Y. Wang, and X. Zhang, "Valley photonic crystals for control of spin and topology," Nat. Mater. **16**, 298 (2017).
7. Z. Wang, Y. Chong, J. D. Joannopoulos, and M. Soljačić, "Observation of unidirectional backscattering-immune topological electromagnetic states," Nature **461**, 772 (2009).
8. Z. Wang, Y. D. Chong, J. D. Joannopoulos, and M. Soljačić, "Reflection-free one-way edge modes in a gyromagnetic photonic crystal," Phys. Rev. Lett. **100**, 013905 (2008).
9. X. Cheng, C. Jouvaud, X. Ni, S. H. Mousavi, A. Z. Genack, and A. B. Khanikaev, "Robust reconfigurable electromagnetic pathways within a photonic topological insulator," Nat. Mater. **15**, 542 (2016).
10. W. J. Chen, S. J. Jiang, X. D. Chen, B. Zhu, L. Zhou, J. W. Dong, and C. T. Chan, "Experimental realization of photonic topological insulator in a uniaxial metacrystal waveguide," Nat. Commun. **5**, 5782 (2014).
11. G. Harder, T. J. Bartley, A. E. Lita, S. W. Nam, T. Gerrits, and C. Silberhorn, "Single-mode parametric-down-conversion states with 50 photons as a source for mesoscopic quantum optics," Phys. Rev. Lett. **116**, 143601 (2016).
12. B. Zhen, C. W. Hsu, L. Lu, A. D. Stone, and M. Soljačić, "Topological nature of optical bound states in the continuum," Phys. Rev. Lett. **113**, 257401 (2014).
13. K. L. Tsakmakidis, A. D. Boardman, and O. Hess, "'Trapped rainbow' storage of light in metamaterials," Nature **450**, 397 (2007).
14. K. L. Tsakmakidis, T. W. Pickering, J. M. Hamm, A. F. Page, and O. Hess, "Completely stopped and dispersionless light in plasmonic waveguides," Phys. Rev. Lett. **112**, 167401 (2014).
15. J. Li, G. Hu, L. Shi, N. He, D. Li, Q. Shang, Q. Zhang, H. Fu, L. Zhou, W. Xiong, J. Guan, J. Wang, S. He, and L. Chen, "Full-color enhanced second harmonic generation using rainbow trapping in ultrathin hyperbolic metamaterials," Nat. Commun. **12**, 6425 (2021).
16. Z. Hayran, H. Kurt, and K. Staliunas, "Rainbow trapping in a chirped three-dimensional photonic crystal," Sci. Rep. **7**, 3046 (2017).
17. C. Lu, C. Wang, M. Xiao, Z. Q. Zhang, and C. T. Chan, "Topological rainbow concentrator based on synthetic dimension," Phys. Rev. Lett. **126**, 113902 (2021).
18. C. Lu, Y. Z. Sun, C. Wang, H. Zhang, W. Zhao, X. Hu, M. Xiao, W. Ding, Y. C. Liu, and C. T. Chan, "On-chip nanophotonic topological rainbow," Nat. Commun. **13**, 2586 (2022).
19. Z. Tian, C. Shen, J. Li, E. Reit, H. Bachman, J. E. Socolar, S. A. Cummer, and T. J. Huang, "Dispersion tuning and route reconfiguration of acoustic waves in valley topological phononic crystals," Nat. Commun. **11**, 762 (2020).
20. G. J. Chaplain, J. M. De Ponti, G. Aguzzi, A. Colombi, and R. V. Craster, "Topological rainbow trapping for elastic energy harvesting in graded Su-Schrieffer-Heeger systems," Phys. Rev. A **14**, 054035 (2020).
21. P. M. Parto, S. Wittek, H. Hodaei, G. Harari, M. A. Bandres, J. Ren, M. C. Rechtsman, M. Segev, D. N. Christodoulides, and M. Khajavikhan, "Edge-mode lasing in 1D topological active arrays," Phys. Rev. Lett. **120**, 113901 (2018).
22. G. Harari, M. A. Bandres, Y. Lumer, M. C. Rechtsman, Y. D. Chong, M. Khajavikhan, D. N. Christodoulides, and M. Segev, "Topological insulator laser: theory," Science **359**, eaar4003 (2018).
23. M. A. Bandres, S. Wittek, G. Harari, M. Parto, J. Ren, M. Segev, D. N. Christodoulides, and M. Khajavikhan, "Topological insulator laser: experiments," Science **359**, eaar4005 (2018).
24. A. Li, W. Chen, H. Wei, G. Lu, A. Alù, C. W. Qiu, and L. Chen, "Riemann-encircling exceptional points for efficient asymmetric polarization-locked devices," Phys. Rev. Lett. **125**, 187403 (2022).
25. X. Shu, A. Li, G. Hu, J. Wang, A. Alù, and L. Chen, "Integrated photonic metasystem for image classifications at telecommunication wavelength," Nat. Commun. **13**, 2123 (2022).
26. Y. Ashida, Z. Gong, and M. Ueda, "Non-Hermitian physics," Adv. Phys. **69**, 249 (2020).
27. L. Sun, B. Zhao, J. Yuan, Y. Zhang, M. Kang, and J. Chen, "Optical resonance in inhomogeneous parity-time symmetric systems," Chin. Opt. Lett. **19**, 073601 (2021).
28. Y. Ao, X. Hu, Y. You, C. Lu, Y. Fu, X. Wang, and Q. Gong, "Topological phase transition in the non-hermitian coupled resonator array," Phys. Rev. Lett. **125**, 013902 (2020).
29. H. Zhao, X. Qiao, T. Wu, B. Midya, and S. Longhi, "Non-Hermitian topological light steering," Science **365**, 1163 (2019).
30. S. Xia, D. Kaltsas, D. Song, I. Komis, J. Xu, A. Szameit, H. Buljan, K. G. Makris, and Z. Chen, "Nonlinear tuning of PT symmetry and non-Hermitian topological states," Science **372**, 72 (2021).
31. K. Wang, A. Dutt, C. C. Wojcik, and S. Fan, "Topological complex-energy braiding of non-Hermitian bands," Nature **598**, 59 (2021).
32. R. El-Ganainy, K. G. Makris, M. Khajavikhan, Z. H. Musslimani, S. Rotter, and D. N. Christodoulides, "Non-Hermitian physics and PT symmetry," Nat. Phys. **14**, 11 (2018).
33. H. X. Wang, G. Y. Guo, and J. H. Jiang, "Band topology in classical waves: Wilson-loop approach to topological numbers and fragile topology," New J. Phys. **21**, 093029 (2019).
34. C. Wang, H. Zhang, H. Yuan, J. Zhong, and C. Lu, "Universal numerical calculation method for the Berry curvature and Chern numbers of typical topological photonic crystals," Front. Optoelectron. **13**, 73 (2020).
35. M. L. Chen, L. J. Jiang, S. Zhang, R. Zhao, Z. Lan, and E. I. Wei, "Comparative study of Hermitian and non-Hermitian topological dielectric photonic crystals," Phys. Rev. A **104**, 033501 (2021).
36. F. D. M. Haldane, "Model for a quantum Hall effect without Landau levels: condensed-matter realization of the 'parity anomaly'," Phys. Rev. Lett. **61**, 2015 (1988).
37. Y. Yang, T. Xu, Y. F. Xu, and Z. H. Hang, "Zak phase induced multiband waveguide by two-dimensional photonic crystals," Opt. Lett. **42**, 3085 (2017).
38. Y. Yang, X. Huang, and Z. H. Hang, "Experimental characterization of the deterministic interface states in two-dimensional photonic crystals," Phys. Rev. Appl. **5**, 034009 (2016).
39. Y. Yang, Y. F. Xu, T. Xu, H. X. Wang, J. H. Jiang, X. Hu, and Z. H. Hang, "Visualization of a unidirectional electromagnetic waveguide using topological photonic crystals made of dielectric materials," Phys. Rev. Lett. **120**, 217401 (2018).